CASL-U-2015-0155-000

VERA Core Simulator Methodology for PWR Cycle Depletion

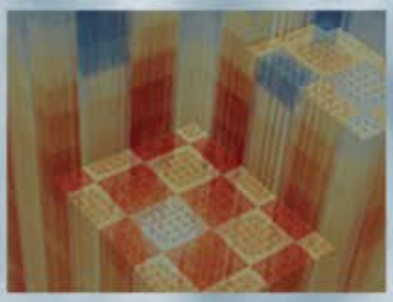

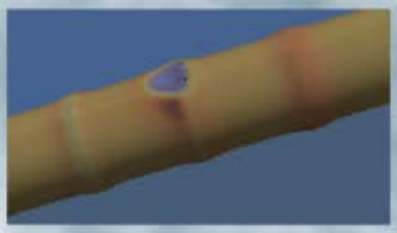

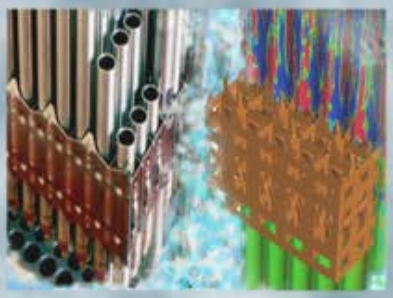

Brendan Kochunas, Daniel Jabaay, Shane Stimpson, Aaron Graham, and Thomas Downar
University of Michigan

Benjamin Collins, Kang Seog Kim, William Wieselquist, Kevin Clarno, and Jess Gehin
Oak Ridge National Laboratory

Scott Palmtag
Core Physics, Inc.

March 29, 2015

CASL-U-2015-0155-000

ANS MC2015 - Joint International Conference on Mathematics and Computation (M&C), Supercomputing in Nuclear Applications (SNA) and the Monte Carlo (MC) Method • Nashville, TN • April 19-23, 2015, on CD-ROM, American Nuclear Society, LaGrange Park, IL (2015)

VERA CORE SIMULATOR METHODOLOGY FOR PWR CYCLE DEPLETION

Brendan Kochunas*[1], Benjamin Collins[2], Daniel Jabaay[1], Shane Stimpson[1], Aaron Graham[1], Kang Seog Kim[2], William Wieselquist[2], Kevin Clarno[2], Scott Palmtag[3], Thomas Downar[1] and Jess Gehin[2]

[1]Department of Nuclear Engineering and Radiological Sciences
University of Michigan

[2]Oak Ridge National Laboratory
1 Bethel Valley Rd., Oak Ridge, Tennessee 37831, USA

[3]Core Physics Inc.

ABSTRACT

This paper describes the methodology developed and implemented in MPACT for performing high fidelity pressurized water reactor (PWR) multi-cycle core physics calculations. MPACT is being developed primarily for application within the Consortium for the Advanced Simulation of Light Water Reactors (CASL) as one of the main components of the VERA Core Simulator, the others being COBRA-TF and ORIGEN. The methods summarized in this paper include a methodology for performing resonance self-shielding and computing macroscopic cross sections, 2-D/1-D transport, nuclide depletion, thermal-hydraulic feedback, and other supporting methods. These methods represent a minimal set needed to simulate high fidelity models of a realistic nuclear reactor. Results demonstrating this are presented from the simulation of a realistic model of the first cycle of Watts Bar Unit 1. The simulation, which approximates the cycle operation, is observed to be within 50 ppm boron (ppmB) reactivity for all simulated points in the cycle and approximately 15 ppmB for a consistent statepoint. The verification and validation of the PWR cycle depletion capability in MPACT is the focus of two companion papers [1,2].

Key Words: MPACT, VERA, CASL

1 INTRODUCTION

One of the main goals of the Consortium for the Advanced Simulation of Light Water Reactors (CASL) [3] is to develop and deliver an enhanced nuclear reactor simulation capability. The traditional approaches to reactor analysis and design have relied on a process involving tools that are not always fully integrated or coupled. Additionally, the neutronics tools are frequently based on nodal diffusion methods which do not preserve the exact problem geometry and approximate neutron transport physics.

To provide an enhanced simulation capability means to provide a high fidelity, pin-resolved, radiation transport capability with the physics for thermal-hydraulics (T-H), fuel pin heat transfer, nuclide transmutation, and corrosion chemistry. It also means that the simulation tools

*Corresponding author: bkochuna@umich.edu; 1906 Cooley Bldg, 2355 Bonisteel Blvd. Ann Arbor, MI 48190

are portable and efficient across a wide range of computer architectures, in particular high performance computing cluster.

A recent paper by Smith and Forget [4] on the high fidelity light water reactor (LWR) neutronics tools provides another perspective on the meaning of "first principles" and "high-fidelity" which gives a good overview of the challenges and requirements that must be met to truly claim an enhanced simulation capability. In broad terms, an enhanced simulation tool should be able to perform isothermal simulations, physics tests, reactivity worth calculations, analysis of cycle depletion, comparison to measured power distributions (e.g. detector responses), and other calculations. All of these requirements must be met while also modeling the fuel rods individually without approximation, and the other support structures (e.g. grid spacers and nozzles) in as much detail as possible. In other work, the application of MPACT has been demonstrated for isothermal problems and start-up physics testing [5] with highly resolved geometry.

This paper focuses on the neutronics capability within CASL and provides an overview of the reactor physics methods developed and implemented in the MPACT code [6] culminating in the application to whole core pressurized water reactor (PWR) cycle depletion. Section 2 presents the methodology for the whole core calculation which includes a summary of the macroscopic cross section calculation, 2-D/1-D transport method, T-H feedback, nuclide depletion and transmutation, along with several supporting methodologies. Section 3 of this manuscript presents a demonstration of these capabilities for a real reactor. The detailed analysis and validation of MPACT's methodology are the focus of two companion papers [1,2]. Finally, Section 4 offers some concluding thoughts and directions for future work.

2 WHOLE CORE CALCULATION METHODOLOGY

2.1 2-D/1-D Transport Method

The 2-D/1-D approach is a numerical method for whole-core transport solutions pioneered largely by the DeCART code [7], but another variation was developed around the same time in the CRX code [8]. Since then, the method has been gaining wider use in the reactor physics community [9,10] and has been demonstrated to provide practical high fidelity solutions [11]. For many practical reactor calculations, the 2-D/1-D method has become popular because its computational costs are considerably lower than those of full 3-D transport. The 2-D/1-D equations approximate the 3-D Boltzmann equation more accurately than the conventional 3-D diffusion equation; they preserve exact transport physics in the radial directions (x and y), but they use diffusion physics in the axial direction (z). The 2-D/1-D equations can be systematically discretized to yield accurate simulation methods for many 3-D reactor core problems. The resulting 2-D/1-D solutions are more accurate than 3-D diffusion solutions, and they are less expensive to generate than standard 3-D transport solutions. The 2-D/1-D equation follows from the 3-D transport equation by modifying the streaming operator with the following approximation:

$$\vec{\Omega}\cdot\nabla\varphi_g\left(\vec{r},\vec{\Omega}\right)\approx\left(\Omega_x\frac{\partial\varphi_g\left(\vec{r},\vec{\Omega}\right)}{\partial x}+\Omega_y\frac{\partial\varphi_g\left(\vec{r},\vec{\Omega}\right)}{\partial y}\right)-\frac{\partial}{\partial z}\frac{D}{4\pi}\frac{\partial\phi_g\left(\vec{r}\right)}{\partial z}, \tag{1}$$

$$\left(\Omega_x \frac{\partial \varphi_g\left(\vec{r},\vec{\Omega}\right)}{\partial x} + \Omega_y \frac{\partial \varphi_g\left(\vec{r},\vec{\Omega}\right)}{\partial y}\right) - \frac{\partial}{\partial z}\frac{D_g\left(\vec{r}\right)}{4\pi}\frac{\partial \phi_g\left(\vec{r}\right)}{\partial z} + \Sigma_{t,g}\left(\vec{r}\right)\varphi_g\left(\vec{r},\vec{\Omega}\right) = q_g\left(\vec{r},\vec{\Omega}\right), \tag{2}$$

To obtain the respective 2-D and 1-D equations, Eq. (2), is integrated in transverse directions. The 2-D equation is obtained by integration of Eq. (2) over a finite interval in *z* and the 1-D axial equation is obtained by integrating Eq. (2) over a finite interval in the *x*-*y* plane. The 2-D equation is given as:

$$\left(\Omega_x \frac{\partial \varphi_g\left(x,y,\vec{\Omega}\right)}{\partial x} + \Omega_y \frac{\partial \varphi_g\left(x,y,\vec{\Omega}\right)}{\partial y}\right) + \Sigma_{t,g,z}\left(x,y\right)\varphi_g\left(x,y,\vec{\Omega}\right) = q_{g,z}\left(x,y,\vec{\Omega}\right) - L_{z,g}\left(x,y,\vec{\Omega}\right), \tag{3}$$

where L_z is the *axial transverse leakage* given by the finite difference approximation of the axial derivative integrated over the interval [*z*-1/2,*z*+1/2], *q* represents the fission and scattering sources, and the subscript *z* denotes that the quantity has been averaged over the axial slice. Similarly, the 1-D equation is:

$$-\frac{\partial}{\partial z} D_{g,x,y}\left(z\right)\frac{\partial \phi_{g,x,y}\left(z\right)}{\partial z} + \Sigma_{t,g,x,y}\left(z\right)\phi_{g,x,y}\left(z\right) = q_{g,x,y,0}\left(z\right) + L_{g,x,y}\left(z\right), \tag{4}$$

Note that in Eq. (4), an integration over $\vec{\Omega}$ has also been performed, but strictly speaking this is not required by Eq. (2). Eqs. (3) and (4) are the typical 2-D/1-D equations solved by MPACT. The details of the solution and discretization of Eq. (3) and Eq. (4) are the focal points of the following sections, respectively. The full description of MPACT's 2-D/1-D method can be found in [12].

2.1.1 2-D Method of Characteristics (MOC)

The 2-D MOC [13] is used to solve the very heterogeneous radial problem and is generally the preferred method for the radial transport in 2-D/1-D because it is capable of treating arbitrary geometry without approximation, scales linearly with the problem size in space, and can be implemented efficiently on a computer. The 2-D transport equation is obtained from the 3-D multi-group Boltzmann transport equation by assuming that the problem has no variation in the axial (*z*) direction. After applying the coordinate transformation the 2-D transport equation in the characteristic direction is:

$$\frac{d}{ds}\varphi_g\left(\vec{r}_{r,0} + s\vec{\Omega}_r, \vec{\Omega}_r\right) + \frac{\Sigma_{t,g}\left(\vec{r}_{r,0} + s\vec{\Omega}_r\right)}{\sin\theta}\varphi_g\left(\vec{r}_{r,0} + s\vec{\Omega}_r, \vec{\Omega}_r\right) = \frac{q_g\left(\vec{r}_{r,0} + s\vec{\Omega}_r, \vec{\Omega}_r\right)}{\sin\theta}, \tag{5}$$

The characteristic's equation is readily solved with integrating factors. Typical discretizations applied to the solution include the discrete ordinates approximation and an isotropic flat source, although deriving and implementing anisotropic and linear sources is straightforward. The transmission equation for the angular flux of group *g* traveling in direction (*m*,*p*) and through region *i* is:

$$\varphi_{i,g,m}^{out} = \varphi_{i,g,m}^{in} \exp\left(-\frac{\Sigma_{t,i,g} s}{\sin\theta_p}\right) + \frac{q_{i,g,m}}{\Sigma_{t,i,g}}\left(1-\exp\left(-\frac{\Sigma_{t,i,g} s}{\sin\theta_p}\right)\right), \tag{6}$$

$$\overline{\varphi}_{i,g,m} = \frac{\varphi_{i,g,m}^{in} - \varphi_{i,g,m}^{out}}{\Sigma_{t,i,g} s_{i,m}} + \frac{q_{i,g,m}}{\Sigma_{t,i,g}}, \tag{7}$$

For reactor applications, the quantity of interest is the scalar flux, which is obtained by integrating the segment averaged angular fluxes of Eq. (7) traversing a given region. The MOC capability in MPACT is fully parallelized in space, angle, and ray, and a complete description of the algorithm is given in [14].

2.1.2 1-D Axial SP_3

To obtain the axial currents needed for the transverse leakage term in radial 2-D MOC equation, a 1-D axial problem must be solved. The 1-D equation given by Eq. (4) can be formulated as a diffusion equation for computational efficiency, although this need not be the case. As an alternative to the diffusion or transport equation the axial solution can be obtained from the simplified P_N (SP_N) equations. In the diffusion equation, the angular flux is assumed to vary linearly in angle. The simplified P_N method assumes an Nth order Legendre expansion for the angular dependence of the angular flux (Eq. 8):

$$\varphi_g(x,\mu) = \sum_{l=0}^{N_{mom}} \frac{2l+1}{2} \varphi_{l,g}(x) P_l(\mu). \tag{8}$$

By substituting this into the transport equation, multiplying by the corresponding Legendre polynomial, and integrating over μ, a system of equations can be constructed. This system of N equations can then be reduced to just the even moment equations. For SP_3, the system of equations is reduced to a system with the 0th and 2nd moments (Eqs. 9 and 10):

$$-\frac{4D_{0,g}}{h^2}\frac{d^2}{d\xi}\Phi_{0,g}(\xi) + \left(\Sigma_{t,g} - \Sigma_{s0,g\to g}\right)\Phi_{0,g}(\xi) = Q_g(\xi) + 2\left(\Sigma_{t,g} - \Sigma_{s0,g\to g}\right)\Phi_{2,g}(\xi), \tag{9}$$

$$\begin{aligned} -\frac{4D_{2,g}}{h^2}\frac{d^2}{d\xi}\Phi_{2,g}(\xi) + \left(\frac{9}{5}\Sigma_{t,g} - \frac{4}{5}\Sigma_{s0,g\to g}\right)\Phi_{2,g}(\xi) \\ = -\frac{2}{5}\left(Q_g(\xi) + 2\left(\Sigma_{t,g} - \Sigma_{s0,g\to g}\right)\Phi_{0,g}(\xi)\right) \end{aligned}, \tag{10}$$

where the dependence on higher-order scattering data is approximated to be zero in the diffusion coefficients, which are defined as:

$$D_{0,g} = \frac{1}{3\Sigma_{tr,g}} \text{ and } D_{2,g} = \frac{9}{35\Sigma_{tr,g}} \tag{11}$$

The SP_N formulation improves, with respect to diffusion, the angular dependence of the discretization, however it is often beneficial to allow for some spatial dependence of the flux. In

this case the nodal expansion method (NEM) [15] is used to define the higher order spatial dependence of the intra-node flux assuming a quadratic expansion for the source and a quartic expansion for the scalar flux.

2.2 T-H Feedback Coupling with COBRA-TF

COBRA-TF (CTF) is a thermal-hydraulic simulation code designed for LWR analysis [16]. CTF includes a wide range of thermal-hydraulic models important to LWR safety analysis including flow regime dependent two-phase wall heat transfer, inter-phase heat transfer and drag, droplet breakup, and quench-front tracking. It uses a two-fluid, three-field representation of the two-phase flow, including continuity of mass, axial and lateral momentum, and energy, by accounting for the liquid, entrained liquid drops, and vapor. This allows CTF to model the axial flow within each channel along with the cross-flow between channels. It also includes several internal models to help facilitate the simulation of actual fuel assemblies, including spacer grid models, a pin conduction model, built-in material properties, and handling non-condensable gas mixtures. The fuel pin model includes radial and azimuthal heat transfer at each axial control volume for each pin location.

The axial mesh for CTF, defined by the user on input, is the basis for coupling with MPACT [17]. The MPACT axial mesh includes the CTF bounds so that the MPACT power (W/m) can be axially- and radially-averaged for each axial slice of each pin location (or water channel) and passed directly to CTF. CTF uses this power in each radial- and azimuthal- control volume for that axial slice and pin location. Because the geometries are identical, energy is conserved. Figure 1 illustrates the pin cell averaged coupling. Note that each code will use a different spatial discretization within a pin cell that is finer then geometric representation, thus the solution transfers require some spatial integration.

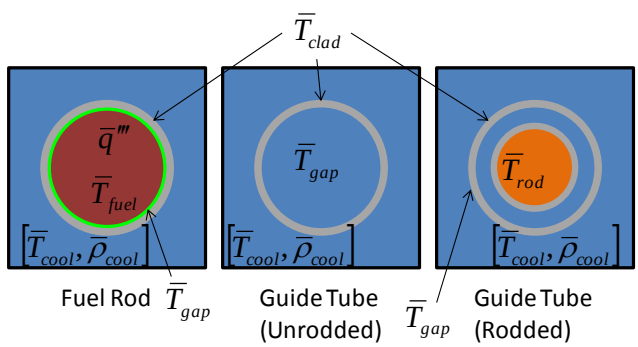

Figure 1. Pin cell coupling models used in MPACT

MPACT requires an average temperature for each radial and azimuthal segment of the fuel, gap, cladding, and coolant, along with an average density for each segment of the coolant. The CTF fuel temperature is averaged over each radial and azimuthal volume of CTF; the gap and cladding are averaged over each azimuthal segment because there are no radial rings in these materials. These values are passed to MPACT and used in all corresponding radial, azimuthal, and axial mesh cells directly. For all four coolant-channels adjacent to a fuel pin, the densities and temperatures are averaged and passed to MPACT for use in all corresponding radial, azimuthal, and axial mesh cells.

CTF is a time-dependent, control volume code that enforces conservation between volumes and is being used within MPACT in a steady-state mode. Internally, CTF uses a pseudo-transient

solver to converge towards a steady-state condition for a particular flow/power state. In a coupled solve, the convergence of the approximate steady-state solution is based on five parameters: global energy, mass balance, fluid energy storage, solid energy storage, and global mass storage. For the work reported in this manuscript, the balance equations are converged to 10^{-6}, and the other terms are converged to 0.005%.

2.3 Nuclide Depletion Coupled with ORIGEN-S

The point depletion calculation is the heart of the depletion capability. It is responsible for solving the differential equation for nuclide transmutation by radioactive decay and nuclear reaction in each discrete spatial region and is given as:

$$\frac{dN_i(t)}{dt} = \sum_{j=1} \ell_{ij} \lambda_j N_j + \bar{\phi} \sum_{k=1} f_{ik} \sigma_{t,k} N_k - (\lambda_i + \sigma_{a,i} \bar{\phi}) N_i, \tag{12}$$

where $N_i(t)$ is the particle number density of nuclide i, λ_i is the radioactive disintegration constant for nuclide i, and σ_a and σ_t are the effective absorption and total cross sections, respectively. The ℓ_{ij} and f_{ik} terms are the branching ratios producing daughter nuclide j by radioactive decay or nuclide k by neutron interaction. The time averaged flux is $\bar{\phi}$.

In MPACT, the solution of Eq. (12) is provided by coupling to ORIGEN-S [22]. In this coupling, ORIGEN-S provides an application program interface (API) to MPACT and the codes are linked together at compile time to avoid excessive file input/output (I/O). The time-stepping algorithm for the depletion calculation in MPACT uses predictor-corrector with sub-stepping as described in [18].

The transport cross section library [19] that is summarized in the next section, does not necessarily contain data for all the fission products needed for the depletion/decay calculation. Therefore, an additional depletion library is used to supplement the transport data when needed. A recently developed depletion library for production calculations with 244 nuclides [20]. However, the full ~2300 nuclide chain standard ORIGEN-S library may also be used. The cross section data for the depletion library are also not necessarily in the same group structure as the transport library, so machinery exists in the coupling of MPACT and ORIGEN-S to map any neutron energy group structure used by the transport calculation to the depletion group structure.

2.4 Macroscopic Cross Section Calculation

The multi-group (MG) MPACT library has been generated from the MG AMPX library, which was prepared by using the AMPX/SCALE code package [21,22] developed at ORNL. The AMPX/SCALE code package includes base MG cross sections and resonance data such as resonance integral and subgroup data. The MPACT code reads the MG MPACT library and generates various reactions of microscopic cross sections for each nuclide at each material zone as needed by which macroscopic cross sections are computed for the diffusion or transport calculations.

The MPACT code is based on the Bondarenko approach including the subgroup [23,24] and embedded self-shielding methods (ESSM) [25,26] for the resonance self-shielding calculation, that provides effective self-shielded cross sections for each nuclide. The subgroup method solves the following fixed-source transport equation to estimate equivalence cross sections ($\Sigma_{e,g}$):

$$\vec{\Omega}_r \cdot \nabla \psi_{g,m} + \sum_i \left(\Sigma_{i,a,g}^m + \lambda_{i,g} \Sigma_{i,p} \right) \psi_{g,m} \left(\vec{\Omega}_r \right) = \sum_i \lambda_{i,g} \Sigma_{i,p} \,, \tag{13}$$

where subscript m denotes a problem case with different absorption cross section levels at energy group g. In Eq. (13), $\Sigma_{i,a,g}$ and $\Sigma_{i,p}$ denote macroscopic absorption and potential cross sections of nuclide i, respectively, and $\lambda_{i,g}$ intermediate resonance parameter. The resultant scalar fluxes can be converted into equivalence cross sections, and thus effective self-shielded cross sections are obtained. The MPACT code includes Wemple's subgroup method [27] for non-uniform temperature profile inside a fuel pin.

Figure 2 illustrates the procedure for updating the macroscopic cross sections in MPACT for the coupled T-H and neutronics calculation. The subgroup fixed source calculations are performed to update the equivalence cross section at each outer iteration due to the T-H update by which macroscopic cross sections including effective fission spectra are updated accordingly. Those updated cross sections are then utilized in the 1-D axial NEM or SP_N, 3-D coarse mesh finite difference (CMFD), and 2-D MOC calculations. The most time consuming part in cross section processing is to perform the 2-D MOC fixed source transport calculation to obtain the equivalence cross section. In order to save memory, typically only equivalence cross sections are saved on memory, and microscopic or macroscopic cross sections are generated as needed.

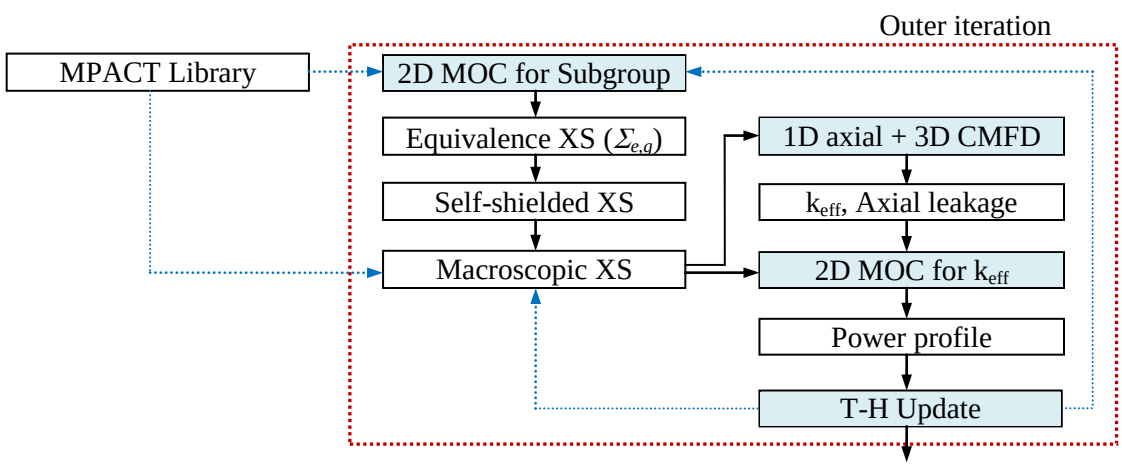

Figure 2. Flow diagram for cross section update

2.5 Supporting Methodologies

2.5.1 Multi-state operational capability

To adequately simulate a cycle of a nuclear reactor, one must account for the operation during that cycle. Normal operation of a reactor includes ramping to full power and powering down, adjusting the feedwater temperature, moving control rod banks, and replenishing soluble boron. In MPACT, a multi-state operational capability exists that allows users to define a sequence of states to capture the operational conditions at a given point in the cycle.

2.5.2 Fuel shuffling and restart for multi-cycle analysis

In the simulation of multiple cycles, one needs to account for the relocation and reuse of fuel assemblies in the reactor. To model the operation of a typical PWR over multiple cycles the

primary shuffling operation is translation, however in the case of a simulation involving symmetry, then rotation of the pins is also required. In addition to the normal cycle-to-cycle shuffling of fuel, there are also extenuating cases in which an assembly may be resident in the spent fuel pool for multiple cycles before returning to the core. There are also rare operational instances in which a fuel assembly is shuffled from another unit. Assemblies with failed rods have also been known to have the failed rod replaced with a dummy rod, and in certain lead test assemblies it is also known that fresh rods have been inserted towards the normal end of life to investigate extremely high burnup regimes.

The shuffling capability in MPACT allows for the translation and rotation (for symmetry) of fuel assemblies as well as shuffling from any given cycle or unit. The shuffle file format uses HDF5 to facilitate portability, data compression, and I/O performance. The typical file size for one core's fuel composition data is just over 2 GB. The file read and write operations support parallel execution. For the write operation all the data that is needed to be written for a given assembly are communicated via a custom non-blocking gather operation, and then the data are written by a single process. The read operation has each process read whatever data it needs directly from the file, avoiding communication. This algorithm enables the composition data for a full core to be written in parallel by a few 1,000 processors in a few minutes. The parallel read, which does not require data aggregation, is executed in fractions of a second for full core calculations.

This feature was verified by comparing the end of cycle pin-wise exposures to their shuffled locations. Figure 3 below shows an example of the simulated pin-wise exposures at the end of cycle (EOC) 1 for Watts Bar Unit 1—the problem presented in Section 3—and the exposures of the shuffled fuel at beginning of cycle (BOC) 2.

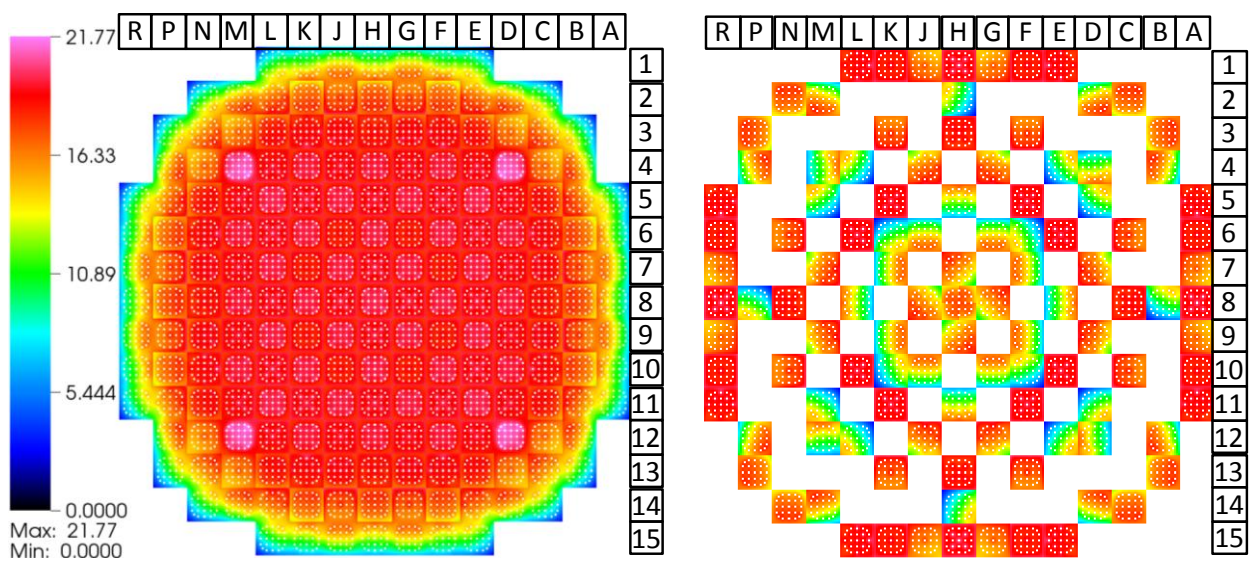

(a) EOC 1 pin-wise exposures **(b) BOC 2 pin-wise exposures**

Figure 3. Watts Bar end of cycle 1 and beginning of cycle 2 exposures

2.5.3 Depletion of B-10 in soluble boron

The depletion of the B-10 isotope is different from all of the other isotopes because the boron is dissolved into the coolant. Both isotopes of boron are present in the soluble boron but the B-10 isotope has a significantly higher neutron absorption cross-section. Without the addition of boron into the system—a scenario which is rare unless the power is significantly decreased—the B-10 concentration in the primary system can be modeled using a simple balance equation. The time rate change in the B-10 isotopes is equal to the difference in the sources and losses of B-10 isotopes. Assuming there are no sources, this differential equation may be written as:

$$\frac{dN_{^{10}B}(t)}{dt} = -N_{^{10}B}(t)\frac{\int_{V_{core}}\int_0^{\infty}\sigma_a^{^{10}B}(E)\phi(\vec{r},E)dEd\vec{r}}{\int_{V_{RCS}} d\vec{r}}. \tag{14}$$

In Eq. (14), V_{RCS} is the volume of the reactor cooling system, which is essentially the primary loop in a PWR. The solution of Eq. (14) can be written in the form of the concentration of B-10 in units of atom % as a function time as shown in Eq. (15).

$$C_{^{10}\mathrm{B}}(\mathrm{t})[\mathrm{at\%}] = C_{^{10}\mathrm{B}}(0)\frac{\exp\left(-t\alpha_{core}\sum_g \sigma_{a,g}^{^{10}B}\bar{\phi}_g\right)}{1-C_{^{10}\mathrm{B}}(0)\left(1-\exp\left(-t\alpha_{core}\sum_g \sigma_{a,g}^{^{10}B}\bar{\phi}_g\right)\right)}. \tag{15}$$

For a Westinghouse 4-loop PWR design α_{core}, the ratio of the core coolant volume to the volume of the primary loop, is estimated to be approximately 5.7%. In MPACT, Eq. (15) is used to estimate the new B-10 fraction in the coolant at every depletion step. Additionally, the B-10 fraction may be specified as part of the VERA input to simulate the addition of new boric acid to the coolant or to better match measured conditions.

2.5.4 Control rod de-cusping

When a control rod is partially inserted into a plane, its tip must be homogenized to eliminate axial heterogeneities within the plane. Because this homogenization results in control rod material throughout the entire plane, it introduces artificially low fluxes around the control rod tip. This error is known as control rod cusping.

In order to reduce the cusping effects, a homogenization correction factor has been implemented in MPACT. This correction factor is unique for each of three control rod materials: AIC, B_4C, and tungsten. For each absorber material, a 3 × 3 assembly case with a control rod in the center assembly was used to quantify the rod cusping effects. It was assumed that the eigenvalue should have changed linearly with rod position. The case was simulated with the control rod tip at seven positions within a plane, and also aligned with the top and bottom of the plane. The k-eff of each simulation was then compared to that of the assumed straight line and used to develop a sixth order polynomial. In MPACT, this polynomial, which has pre-generated coefficients based on rod type, is used to adjust the volume fraction of the control rod material to minimize the reactivity error of the rod cusping effects.

3 WATTS BAR CYCLE 1 SIMULATION

As mentioned previously, the focus of this paper is primarily on summarizing the methods and capability, rather than the results. Detailed simulation results for public benchmarks are the focus of two companion papers [1,2], and some simulation results and computational performance are discussed herein. The focus of this section is the public Watts Bar model described in [28]: specifically the VERA benchmark progression problem 9. The core loading pattern from cycle 1 is illustrated Figure 4.

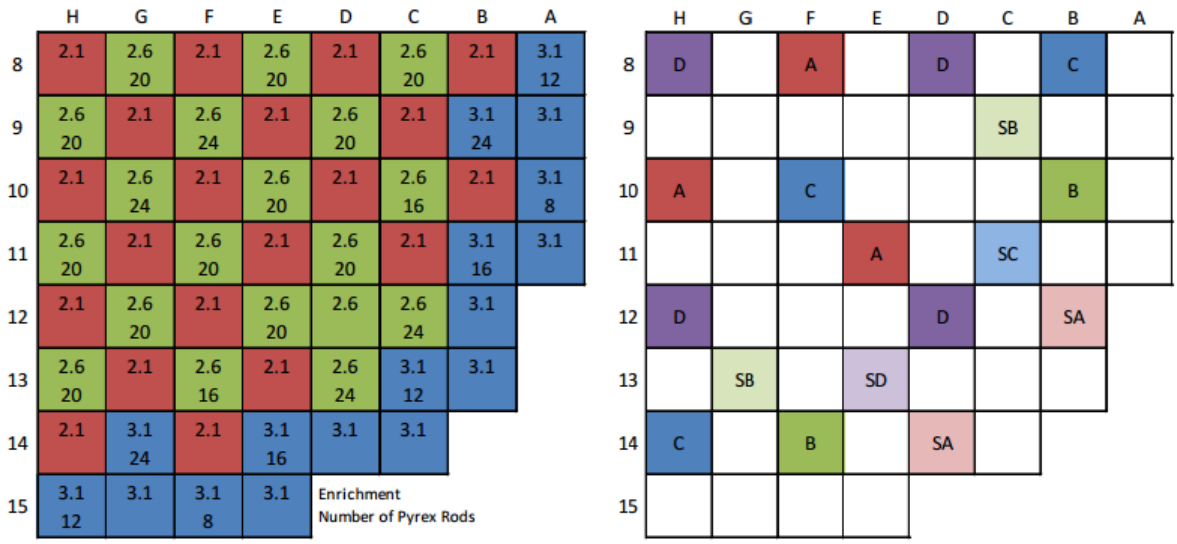

Figure 4. Watts Bar cycle 1 public assembly, poison, and control rod layout [28]

The operational history of the reactor is approximated due to its complexity. The simulated history used in this calculation is given in Table I, and the detailed history of the operation is illustrated in [28]. The approximations include constant power that preserves the integral power over the cycle excluding the ramp-up and coast-down, and constant rod position.

For the MOC discretization the Chebyshev-Gauss quadrature was used with 16 azimuthal angles per octant and 4 polar angles per octant and a ray spacing of 0.05 cm. Transport corrected P_0 based on neutron leakage conservation [29] with the out-scatter approximation was used for the scattering treatment. The cross section library used by MPACT is a 47-group library generated by ORNL and described in detail in [19]. For the thermal-hydraulics in CTF, the direct-moderator heating fraction was set to 2% and the heat transfer coefficient for the fuel-clad gap was set to 10,000 W/m^2-K as this was observed to give good agreement for the core average temperature compared to conventional methods.

The simulation was performed on the Eos compute cluster [30], which is a Cray XC30 with 744 physical nodes, with each node containing two 8-core 2.6 GHz Intel Xeon E5-2670 processors with available hyper-threading and 64 GB of RAM. The problem was decomposed in MPACT with 2378 spatial domains (58 axial and 41 radial) and 2 hyper-threads for a total of 4756 processors. CTF used 56 of these processors for assembly decomposition. It was

determined that the 41 radial domains are more suitable than the 46 domains that have been used in several previous calculations because the maximum subdomain size in either case is the same (1.5 assembly × 1.5 assembly).

The results are provided in Figure 4 and in Table I below. Reasonable agreement with measurement is observed, although there are still notable differences. From the results in Figure 4 the only direct points of comparison are the HZP state and the 32 EFPD exposure case. The HZP case agreement is consistent with previous results [5] while the result for the 32 EFPD state has reasonably good comparison to measurement with a difference of 16.21 ppmB. Most of the rest of the simulated points appear to differ within 50 ppmB of measurement as noted by the black dashed lines in Figure 5. The typical acceptance criteria PWR reactivity surveillance is 50ppmB, therefore observing reactivity differences within 50 ppmB is deemed reasonable at this stage of development for VERA-CS given the known modeling and methods approximations.

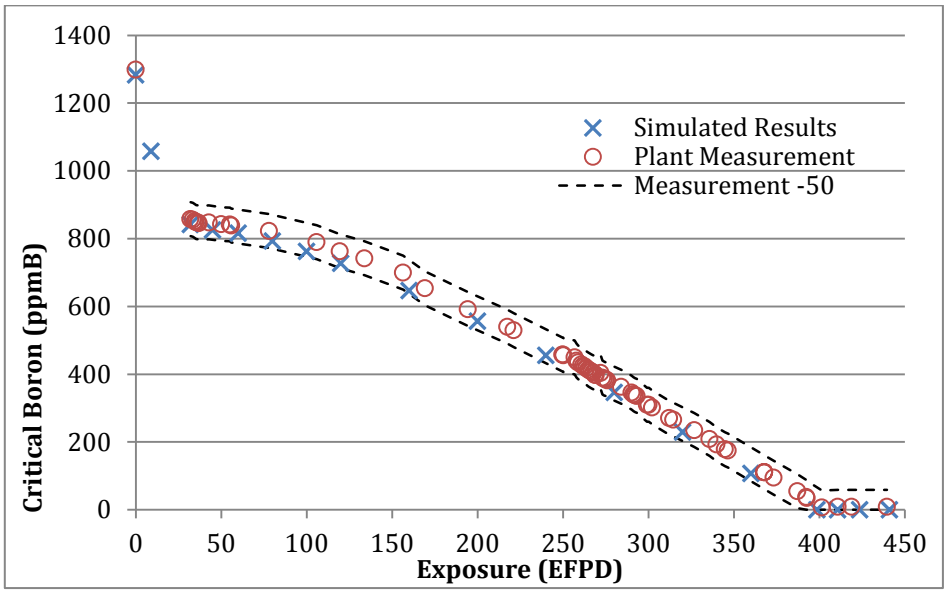

Figure 5. Predicted critical boron concentration for Watts Bar cycle 1

The observed differences in the predicted reactivity are attributed primarily to either the approximations in operation or the predicted fuel temperature. As mentioned before, the fuel-clad gap is treated with a constant heat transfer coefficient that is spatially-uniform in the core for the entire cycle. This prediction of the heat transfer across the fuel-clad gap is extremely important to the prediction of the fuel temperature and overall reactivity. The heat transfer across this gap can affect the fuel temperature by as much as 300 °K, and typical Doppler reactivity worth for UO_2 is ~2 pcm/°K. Meanwhile the direct moderator heating fraction can only account for ~10 °K. The addition of a more accurate gap conductance model is an area of future work.

The total simulation time was approximately 28 hours (27:57:34) for 19 states: the average solve time per state being 88 minutes and 37 seconds. Of the total simulation time 33% was spent in the COBRA-TF solve, 12% was spent performing the resonance subgroup calculation, 2% was spent in the depletion solve, and 53% of the time was spent in MPACT solving the transport equation.

Table I. Cycle 1 simulated and measured operation history

Simulated					Measured			
Exposure (EFPD)	Power (%)	Bank D	Boron (ppmB)	Avg. Fuel Temp (K)	Exposure (EFPD)	Power (%)	Bank D	Boron (ppmB)
0	1.0E-6	186	1283	291.7	0.0	0	186	1299
9	65.7	219	1058	756.9	---	---	---	---
32	99.7	219	842	873.4	32.0	99.7	219	858
45	97.7	219	826	866.0	42.8	100	215	848
60	97.7	219	816	865.8	55.9	99.9	214	839
80	97.7	219	793	865.3	78.0	99.9	208	823
100	97.7	219	762	864.8	105.8	99.8	217	790
120	97.7	219	727	864.4	119.4	99.8	212	763
160	97.7	219	647	863.6	156.4	99.9	218	700
200	97.7	219	557	862.8	194.3	98.9	215	592
240	97.7	219	456	862.1	249.6	99.9	216	458
280	97.7	219	346	861.4	284.0	99.9	218	363
320	97.7	219	229	860.9	314.5	99.5	214	266
360	97.7	219	107	860.5	367.7	100	216	111
398.6	97.7	219	1.0E-07	860.1	401.4	99.6	217	7
410.7	89.9	219	1.0E-07	833.3	410.7	89.9	216	9
423.6	78.8	219	1.0E-07	796.0	418.8	83.4	228	9
441	64.5	219	1.0E-07	750.0	439.5	65.3	227	9

4 CONCLUSIONS

An overview of the methodology in MPACT that enables simulation of a PWR through multiple cycles was presented. The description of this methodology was given from the point of view of a neutronics core simulator. The methods described included the 2-D/1-D iterative scheme for solving the transport equation efficiently for the whole core. The calculation and depletion capabilities were also summarized. The coupling to COBRA-TF for T-H feedback and the calculation of macroscopic cross sections were also discussed. Supporting methods for the reactor operation, control rod cusping, B-10 depletion, and fuel shuffling were also briefly summarized. The culmination of these methods into a capability for PWR cycle depletion was demonstrated using the VERA Benchmark problem 9 for Watts Bar Unit 1 Cycle 1. The comparison to measurement in this simulation was reasonable with the overall reactivity being predicted within 50 ppmB of measurement, and being quite good for cases with consistent conditions. The observed differences are suggested to be caused by a combination of model approximations and the absence of a robust gap conductance model. Continued investigation into addressing resolving these differences is an area of future work.

To achieve this goal, the future work will focus on adding a gap conductance model, and accounting for thermal expansion. Run time improvements can also be made which would allow for less approximation in the cycle operating history. In addition to these items effort will be made to add capability to MPACT to allow for its application to a wider range of problems including those related to Chalk River unidentified deposits (CRUD) where the CRUD layer is

explicitly tracked and the CRUD source term is obtained from coupling with a chemistry code. CASL also has plans to increase functionality of MPACT for application to BWRs.

5 ACKNOWLEDGEMENTS

This research was supported by the Consortium for Advanced Simulation of Light Water Reactors (www.casl.gov), an Energy Innovation Hub (http://www.energy.gov/hubs) for Modeling and Simulation of Nuclear Reactors and also made use of resources of the Oak Ridge Leadership Computing Facility at the Oak Ridge National Laboratory, which is supported by the U.S. Department of Energy under Contract No. DE-AC05-00OR22725.

6 REFERENCES

1. B. Collins and A.T. Godfrey, "Analysis BEAVRS Benchmark using VERA-CS," *Proc. M&C & SNA 2014*, Nashville, TN, USA. April 19-23 (2014).
2. A.T. Godfrey, et al., "VERA-CS Solutions to the CASL Core Physics Benchmark Progression Problems," *Proc. M&C & SNA 2014*, Nashville, TN, USA. April 19-23 (2014).
3. "Consortium for Advanced Simulation of Light Water Reactors (CASL)", http://www.casl.gov, (2014).
4. K. Smith and B. Forget, "Challenges in the Development of High Fidelity LWR Core Neutronics Tools," *Proc. M&C 2013*, Sun Valley, ID, USA. May 5-9 (2013).
5. A.T. Godfrey, "MPACT Testing and Benchmarking Results," *CASL-U-2014-0045-000*, Oak Ridge National Laboratory, http://www.casl.gov/docs/CASL-U-2014-0045-000.pdf, (2014).
6. B. Kochunas, et al., "Overview of Development and Design of MPACT: Michigan Parallel Characteristics Transport Code," *Proc. M&C 2013*, Sun Valley, ID, USA. May 5-9 (2013).
7. H.G. Joo, J.Y. Cho, et al., "Methods and performance of a three-dimensional whole core transport code DeCART," *Proc. PHYSOR 2004*, Chicago, IL, USA. April 25-29 (2004).
8. N.Z. Cho, G.S. Lee, and C.J. Park, "Fusion Method of Characteristics and Nodal Method for 3D Whole Core Transport Calculation," *Trans. Am. Nucl. Soc.*, **86**, pp. 322-324 (2002).
9. F. Févotte and B. Lathuilière, "MICADO: Parallel Implementation of a 2D-1D Iterative Algorithm for the 3D Neutron Transport Problem in Prismatic Geometries," *Proc. M&C 2013*, Sun Valley, ID, USA. May 5-9 (2013).
10. A. Marin-Lafleche, M.A. Smith, and C. Lee, "PROTEUS-MOC: A 3D Deterministic Solver Incorporating 2D Method of Characteristics," *Proc. M&C 2013*, Sun Valley, ID, USA. May 5-9 (2013).
11. Y.S. Jung, et al., "Practical numerical reactor employing direct whole core neutron transport and subchannel thermal/hydraulic solvers", *Ann. Nucl. Energy*, **62**, pp. 357-374 (2013).
12. B. Collins, et al., "Three-Dimensional Nuclear Reactor Simulations of the Boltzmann Transport Equation with the 2D/1D Method Using MPACT," *Journal of Comp. Phys.*, (in preparation, 2015).
13. M.J. Halsall, "CACTUS, A Characteristics Solutions to the Neutron Transport Equations in Complicated Geometries," AEEW-R-1291, U.K. Atomic Energy Authority (1980).

14. B. Kochunas, "A Hybrid Parallel Algorithm for the 3-D Method of Characteristics Solution of the Boltzmann Transport Equation on High Performance Compute Clusters", *PhD Dissertation*, University of Michigan, http://deepblue.lib.umich.edu/handle/2027.42/100072 (2013).

15. H. Finnemann, F. Bennewitz, and M. Wagner, "Interface Current Techniques for Multidimensional Reactor Calculations," Atomkernenergie, 30, 123 (1977).

16. M. N. Avramova, "CTF: A Thermal Hydraulic Sub-Channel Code for LWR Transient Analyses, User's Manual," Pennsylvania State University, Department of Nuclear Engineering (2009).

17. B. Kochunas et al., "Operational Reactor Depletion Analysis Capability," *CASL-U-2014-0189-000*, Oak Ridge National Laboratory (2014).

18. A. Zhu, et al., "Assessment of the Depletion Capability in MPACT," *Proc. PHYSOR 2014*, Kyoto, Japan, Sept. 28 – Oct. 3 (2014).

19. K. S. Kim, et al., "Development of a New 47-group Library for the CASL Neutronics Simulators," *Proc. M&C & SNA 2014*, Nashville, TN, USA. April 19-23 (2014).

20. W. Wieselquist, "The SCALE 6.2 ORIGEN API for High Performance Depletion," *Proc. M&C & SNA 2014*, Nashville, TN, USA. April 19-23 (2014).

21. D. Wiarda, S. Goluoglu, M.E. Dunn, N.M. Green and L. M. Petrie, "AMPX-6: A Modular Code System for Processing ENDF/B Evaluations," in process (2015).

22. SCALE: A Modular Code System for Performing Standardized Computer Analyses for Licensing Evaluation, ORNL-TM/2005/39, Version 6, Vols. I–III, Oak Ridge National Laboratory, Oak Ridge, Tenn. (2009).

23. A. Khairallah and J. Recolin, "Calcul de l'autoprotection résonnante dans les cellules complexes par la méthode des sous-groupes," *Proc. Seminar IAEA-SM-154 on Numerical Reactor Calculation*s, pp 305-317, I.A.E.A., Vienna (1972).

24. R. J. J. Stamm'ler et al., "The HELIOS Methods," Studsvik Scandpower (1998).

25. S.G. Hong and K.S. Kim, "Iterative Resonance Treatment Methods Using Resonance Integral Table in Heterogeneous Transport Lattice Calculations," *Ann. Nucl. Energy*, **38**, pp. 32-43 (2011).

26. Mark L. Williams and Kang-Seog Kim, "The Embedded Self-Shielding Method," *PHYSOR 2012*, Knoxville, Tennessee, USA, April 15-20, 2012 (2012).

27. C.A. Wemple, et al., "Improved Temperature-Dependent Resonance Treatment in HELIOS-1.9," *Trans. Am. Nucl. Soc.*, **96**, pp. 657-659 (2007).

28. A.T. Godfrey, "VERA Core Physics Benchmark Progression Problem Specifications," *CASL-U-2012-0131-004*, Rev. 4, Oak Ridge National Laboratory, Aug. 29 (2014).

29. B. R. Herman, et al., "Improved Diffusion Coefficients Generated From Monte Carlo Codes," *Proc. M&C 2013*, Sun Valley, Idaho, May 5-9 (2013).

30. Oak Ridge Leadership Computing Facility, "Eos User Guide", (2014), http://www.olcf.ornl.gov/support/system-user-guides/eos-user-guide/.